

## Materials Science inc. Nanomaterials &amp; Polymers

Low-Temperature Sn<sup>0</sup> Nanoparticles Synthesis by Means of Tin(II) N,N-Complexes ReductionMichael Srb,<sup>[a]</sup> Yaraslava Milasheuskaya,<sup>[a]</sup> Roman Jambor,<sup>[a]</sup> Kateřina Kopecká,<sup>[a, b]</sup> and Petr Knotek<sup>\*[a]</sup>

A novel low-temperature liquid phase synthesis of the Sn<sup>0</sup> nanoparticles has been reported. The effect of different reducing agents (Li[AlH<sub>4</sub>], K[BET<sub>3</sub>H], Na[BH<sub>4</sub>]) on the reduction of the two different N,N-coordinated Sn<sup>II</sup> complexes has been described. The influence of the different imino-pyridine chelating ligands to the synthesis of the Sn<sup>0</sup> particles, their separation

and the usage of surfactant for resuspension to nanocolloid has been studied. The Sn<sup>0</sup> nanoparticles were studied by means of Energy-dispersive X-ray spectroscopy, powder X-ray diffraction, atomic force microscopy and dynamic light scattering from the point of view of the chemical composition, crystallinity and size/agglomeration behavior.

## Introduction

Tin containing alloy was the first metallic alloy developed and widely used by mankind for thousands of years before our era. In modern times, tin-based eutectic alloy with lead (63 wt.% of Sn with the melting point 183 °C) was frequently used for soldering due to the strength of the joint, as well as due to the conserved chemical composition which is stable at all the used atmospheric conditions and, thanks to a low operating temperature, prevented thermal damage of the devices concerned. Pb-containing alloys are banned, however, by the Restriction of Hazardous Substances Directive 2002/95/EC.<sup>[1]</sup> As a consequence, Pb-free soldering became one of the most interesting topics in material science at the beginning of the millennium due to the solder material market size of over 1 billion USD.<sup>[1b,c,2]</sup> Tin-based materials are still widely studied but attention has moved from tin alloys to tin nanoparticles because of the possibility of decreasing the melting temperature with a reduction of particle size ( $T_{\text{melting}}$  140 °C for the sub 10 nm Sn-nanoparticles<sup>[3]</sup> is lower than the original Sn–Pb eutectic solder;  $T_{\text{melting}}$  230 °C for the bulk Sn). The possible applications of tin nanoparticles are therefore not limited to soldering. They have also been widely studied as an anode material for Li-battery technology,<sup>[4]</sup> for catalytical purposes e.g. for alkylation,<sup>[5]</sup> production of the conductive inks,<sup>[3a]</sup> alternative route for planar waveguide preparation by local glass Sn-enrichment instead of the expensive Sn ion-implantation<sup>[6]</sup> for solarization

of glass surfaces and increasing the second harmonic generation effect and holographic recording in glasses.<sup>[7]</sup>

The Sn-based nanoparticles can be prepared via both top-down or bottom-up approaches. As an example of a top-down approach from bulk metal, one can name high-intensity ultrasound treatment,<sup>[8]</sup> the spark erosion method<sup>[9]</sup> or the surfactant-assisted solution plasma technique.<sup>[10]</sup> The ablation method, the next top-down method for the preparation of metallic nanoparticles,<sup>[11]</sup> was used for the Ge–Sn alloy or SnO<sub>x</sub> nanoparticles.<sup>[12]</sup> The tin nanoparticles resulting from the procedures mentioned above are nearly spherical but with a large size distribution (e.g. 50–3500 nm<sup>[8]</sup>). More precise control of the Sn<sup>0</sup> nanoparticles size was achieved by the bottom-up approach. Nanoparticles can be prepared by a hydrothermal synthesis in H<sub>2</sub> atmosphere or the microwave-assisted solvothermal route,<sup>[4a,13]</sup> but the most promising procedure is the chemical reduction. The strong influence on the properties of final nanoparticles has been reported for different reduction agents (e.g. diethylene glycol,<sup>[14]</sup> Na[BH<sub>4</sub>],<sup>[3a,15]</sup> K[BH<sub>4</sub>],<sup>[16]</sup> NaH,<sup>[17]</sup> n-BuLi<sup>[18]</sup> or KC<sub>8</sub><sup>[19]</sup>). Equally important is the role of the precursors,<sup>[14]</sup> complexing agents modifying the reaction route (e.g. 1,10 N,N-phenantroline<sup>[15b,20]</sup>), or surfactants for the stabilization of the colloid.<sup>[15b,20–21]</sup> The thermal decomposition of organometallic complexes was also tested as an alternative route for Sn<sup>0</sup> nanoparticles preparation e.g. [[Sn(NMe<sub>2</sub>)<sub>2</sub>]<sub>2</sub>] at 140 °C,<sup>[22]</sup> [Sn(salen)] at 650 °C<sup>[4b]</sup> or Bu<sub>3</sub>SnPh (tributylphenyltin) at 700 °C.

We were focused in this study on a room temperature Sn<sup>0</sup> nanoparticles preparation route. Two imino-pyridines L<sup>1,2</sup> were used to prepare N,N-coordinated complexes [L<sup>1,2</sup>→SnCl<sub>2</sub>]. Subsequent substitution yielded unstable complexes [L<sup>1,2</sup>→SnH<sub>2</sub>] *in situ* that eliminated the molecule of H<sub>2</sub> easily along with the syntheses of the desired Sn<sup>0</sup> nanoparticles.<sup>[23]</sup> The influence of different chelating ligands L<sup>1,2</sup>, the use of different reduction agents as well as the addition of surfactant on the properties of the resulting Sn<sup>0</sup> nanoparticles were studied.

[a] M. Srb, Y. Milasheuskaya, Prof. R. Jambor, Ing. K. Kopecká, Ing. P. Knotek  
Department of General and Inorganic Chemistry  
Faculty of Chemical Technology, University of Pardubice  
Studentská 573, 532 10 Pardubice, Czech Republic  
E-mail: petr.knotek@upce.cz

[b] Ing. K. Kopecká  
Center of nano structured polymers SYNPO, a.s.  
S. K. Neumanna 1316, 532 07 Pardubice, Czech Republic

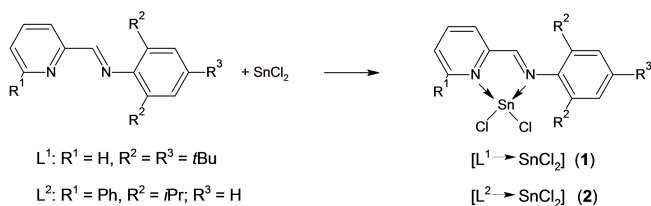
Supporting information for this article is available on the WWW under  
<https://doi.org/10.1002/slct.202100618>

## Results and Discussion

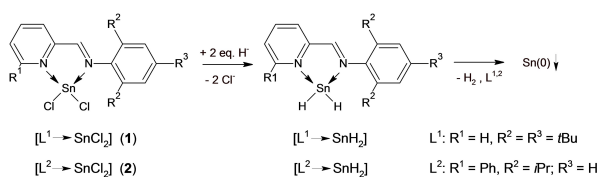
Chelating ligands  $L^{1,2}$  were prepared according to the literature procedure.<sup>[24]</sup> Treatment of  $L^{1,2}$  with 1 eq. of  $\text{SnCl}_2$  provided the starting  $N,N$ -chelated complexes  $[L^1 \rightarrow \text{SnCl}_2]$  (1) and  $[L^2 \rightarrow \text{SnCl}_2]$  (2), respectively (Scheme 1).

Compounds 1 and 2 are highly soluble in chlorinated solvents. Both compounds have been characterized by elemental analysis and NMR spectroscopy (see Supplementary materials). In the  $^1\text{H}$ NMR spectrum of 1 the  $\text{CH}=\text{N}$  proton resonates at  $\delta = 8.39$  ppm shifted downfield as compared to the starting ligands  $L^1$  ( $\delta = 8.21$  ppm, similarly  $\delta = 8.69$  ppm for 2 vs.  $\delta = 8.37$  ppm for  $L^2$ ). The  $^1\text{H}$ NMR spectrum of 1 revealed a downfield shift of hydrogen in the *ortho* position of the pyridine ( $\delta = 9.29$  ppm) as compared with free  $L^1$  ( $\delta = 8.67$  ppm). The  $^{119}\text{Sn}$  NMR spectrum of 1 revealed signal  $-219.5$  ppm ( $\delta = -235.5$  ppm for 2). The values are shifted upfield when compared to the related complex  $[\text{TMEDA} \rightarrow \text{SnCl}_2]$  ( $\delta = -165.0$  ppm)<sup>[25]</sup> suggesting higher electronic shielding of the tin atom in 1 and 2 due to the strong  $\text{CH}=\text{N} \rightarrow \text{Sn}$  coordination. In addition, the tin atom is sterically protected by *t*Bu groups of the  $\text{CH}=\text{N}$  moiety in 1, while the shielding of the Sn atom is arranged by the Ph group in the *ortho* position of the pyridine in 2.

Complexes 1 was used as the starting material for the production of the  $\text{Sn}^0$  nanoparticles at laboratory temperature. The addition of the stoichiometric amount of hydride originated from  $\text{Li}[\text{AlH}_4]$ ,  $\text{K}[\text{BEt}_3\text{H}]$  or  $\text{Na}[\text{BH}_4]$  to the solution of 1 provided the unstable  $N,N$ -chelated complex  $[L^1 \rightarrow \text{SnH}_2]$ . We used reducing agents that significantly differ from the reactivity as illustrated e.g. by decomposition temperature/decomposition enthalpy per one hydrogen atom  $180^\circ\text{C}/22 \text{ kJ}\cdot\text{mol}^{-1}$  and  $400^\circ\text{C}/-47 \text{ kJ}\cdot\text{mol}^{-1}$  for  $\text{Li}[\text{AlH}_4]$  and  $\text{Na}[\text{BH}_4]$ , respectively.<sup>[26]</sup> A spontaneous redox reaction provided the  $\text{Sn}^0$  nanoparticles along with the elimination of  $\text{H}_2$  and free ligand  $L^1$  as detected by the  $^1\text{H}$ NMR spectrum of the crude reaction mixture (Scheme 2).



Scheme 1. Synthesis of compounds 1 and 2.



Scheme 2. The general reaction pathway for  $\text{Sn}^0$  formation.

The separated dried product was a gray, crystal-like solid material with the size of hundreds of  $\mu\text{m}$  illustrated in Figure 1. The materials were agglomerates of smaller particles (see Figure 1 and Figure S8). The chemical composition responds to the Sn with a typical content 96 wt.% (Figure 2a). The traces of Al (the rest of the reagents), Si (the fragments of the chemical

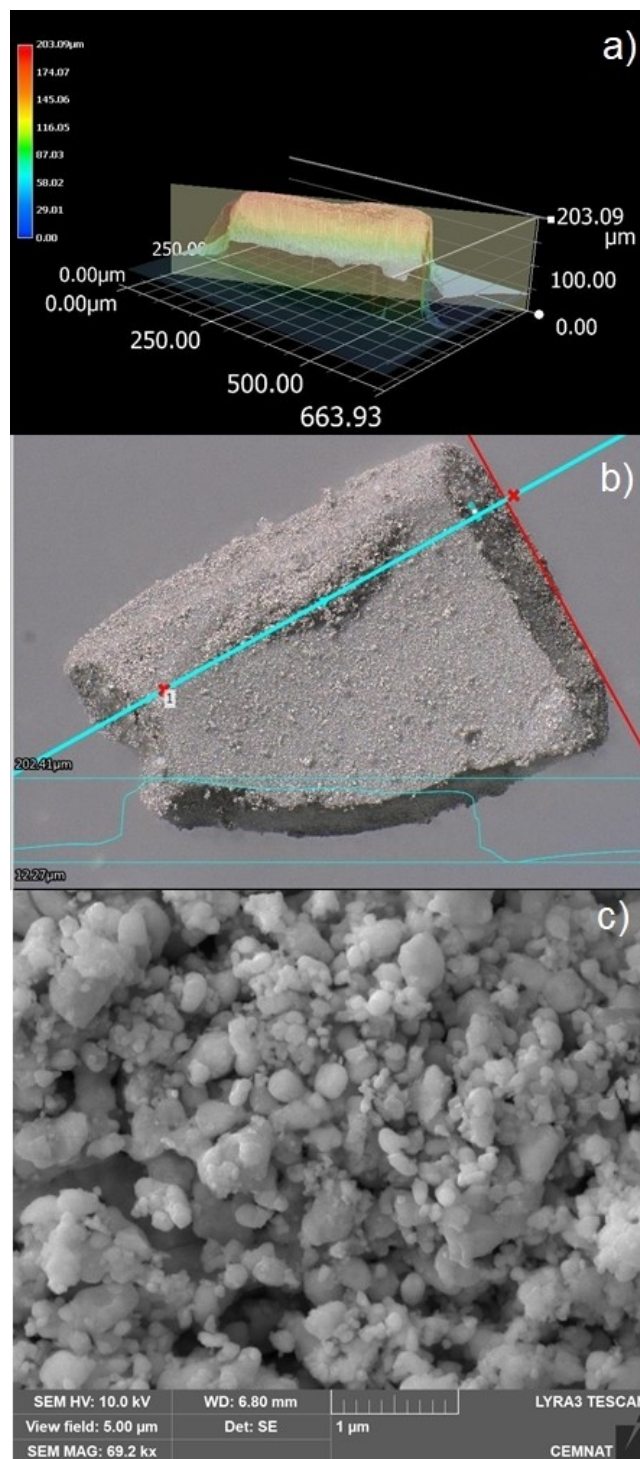
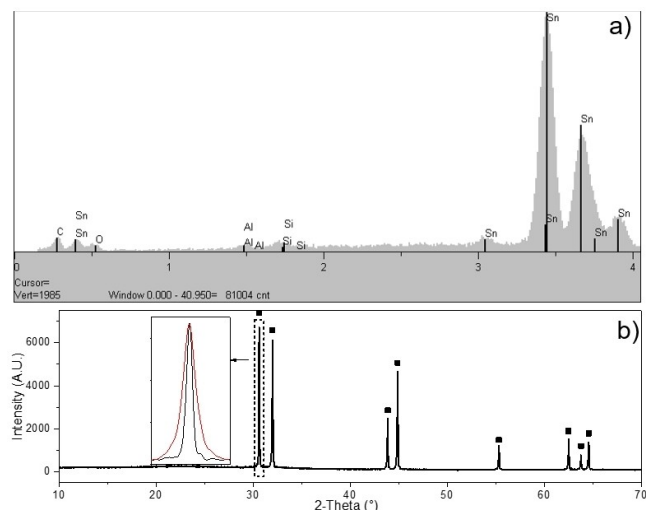


Figure 1. Optical (a, b) and SEM (c) microscopic images of the formed  $\text{Sn}^0$  solids originated/resulted from the reaction 1 +  $\text{Li}[\text{AlH}_4]$ .



**Figure 2.** (a) Illustration of EDX spectra and (b) XRD pattern of the Sn<sup>0</sup> particles originated from the reaction 1 + Li[AlH<sub>4</sub>] (black); the inset shows the difference of the full-width of the diffractions in comparison to the product of 1 + Na[BH<sub>4</sub>] (red).

apparatus) and routine/unexceptional traces of carbon and oxygen (C target for the sample and surface contamination) were detected (Figure 2).

The samples were characterized by the powder X-ray diffraction (XRD). Figure 2b indicates the XRD patterns of the as-prepared material. All diffraction peaks can be readily indexed to crystalline tin with tetragonal lattice (JCPDS card No. 04-004-6229, see black squares and Figure S9). No peak belonging to the other crystalline compounds was detected. The Scherrer formula<sup>[27]</sup> was applied for the calculation of the average crystallite size based on the calculation of full pattern matching using EVA software.<sup>[28]</sup>

The Sn<sup>0</sup> that was prepared by the reduction of 1 was dispersed in the THF and sonicated for 25 minutes. The material was broken up into the colloidal system, which seems to be stable without the occurrence of any sediment. The hydrodynamic size of the particles was determined by the DLS and the histograms of the hydrodynamic diameters are illustrated in Figure 3 for all the reducing agents. For all the reduction agents, the histogram was bimodal. "Small" fractions have been located in a range of 50–160 nm, where the lowest fraction was prepared by the reaction of 1 with K[BEt<sub>3</sub>H]. This fact frequently influenced the effective hydrodynamic diameter of the colloid ( $D_H$  eff), but non-precisely, used as the main parameter of particle size,<sup>[29]</sup> see the data in Tab. 1. In addition, the size of the crystallite (XRD) is comparable with the "small" fraction of colloid for the Sn<sup>0</sup> obtained by the reaction of 1 with K[BEt<sub>3</sub>H]. From this point of view, the size of the Sn<sup>0</sup> depends on the reduction agent and the K[BEt<sub>3</sub>H] is the best reagent.

The reaction of 2 with K[BEt<sub>3</sub>H] has therefore been done and the decomposition of an unstable [L<sup>2</sup>→SnH<sub>2</sub>] provided the Sn<sup>0</sup> (Scheme 2), which has been separated and characterized in a similar manner. The data obtained both from the crystallite (XRD) and THF dispersion (DLS) are provided in Table 1 and

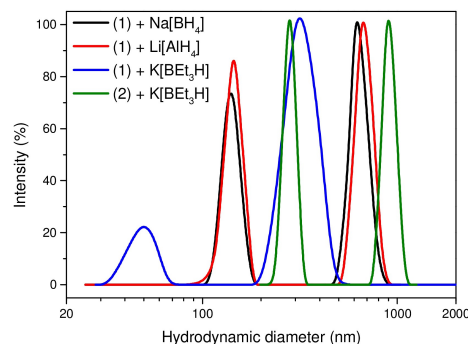


**Figure 3.** The Sn<sup>0</sup> particles' colloidal size distribution analyzed by the DLS after 25 min sonication in THF.

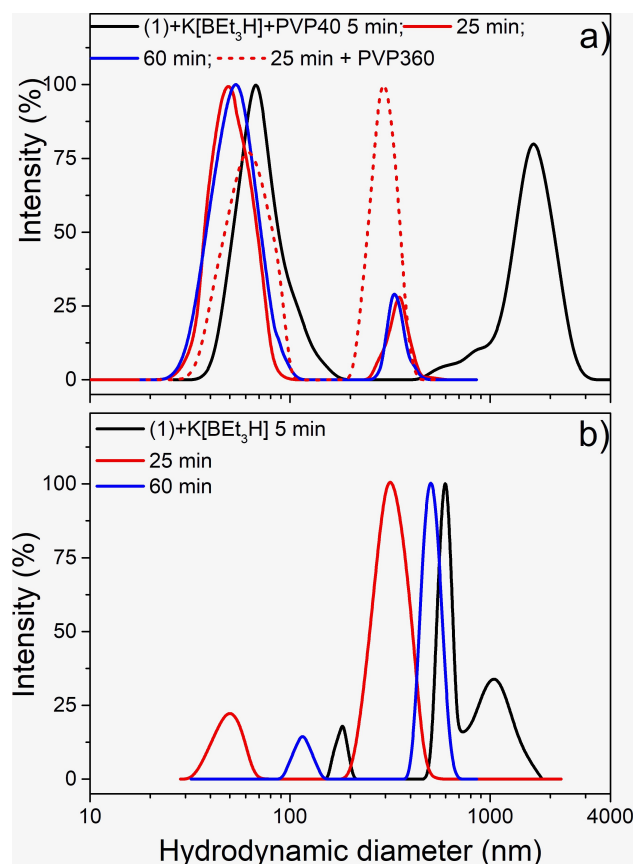


**Figure 4.** The particle size distribution of the Sn<sup>0</sup> dispersed via bath sonication for different times of sonication: as prepared (a), stabilized by PVP (b). The measurements were taken directly after sonication in THF.

Figure 3. It is apparent that the use of ligand L<sup>2</sup>, where the Sn atom is protected by the *Ph* in the *ortho* position of the pyridine, provided the material with significantly higher crystallite and size of the "small" fraction as compared to ligand L<sup>1</sup> (Table 1). The size of the Sn<sup>0</sup> may also be tuned by sterical shielding of the ligand L. Our results suggest an important role of the substituents on the CH=N group (compare 2,4,6-*t*Bu<sub>3</sub>-C<sub>6</sub>H<sub>2</sub> in L<sup>1</sup> vs. 2,6-*i*Pr<sub>2</sub>-C<sub>6</sub>H<sub>3</sub> in L<sup>2</sup>) and the negligible effect of the *ortho* substituents of pyridine (compare *H* in L<sup>1</sup> vs. *Ph* in L<sup>2</sup>).

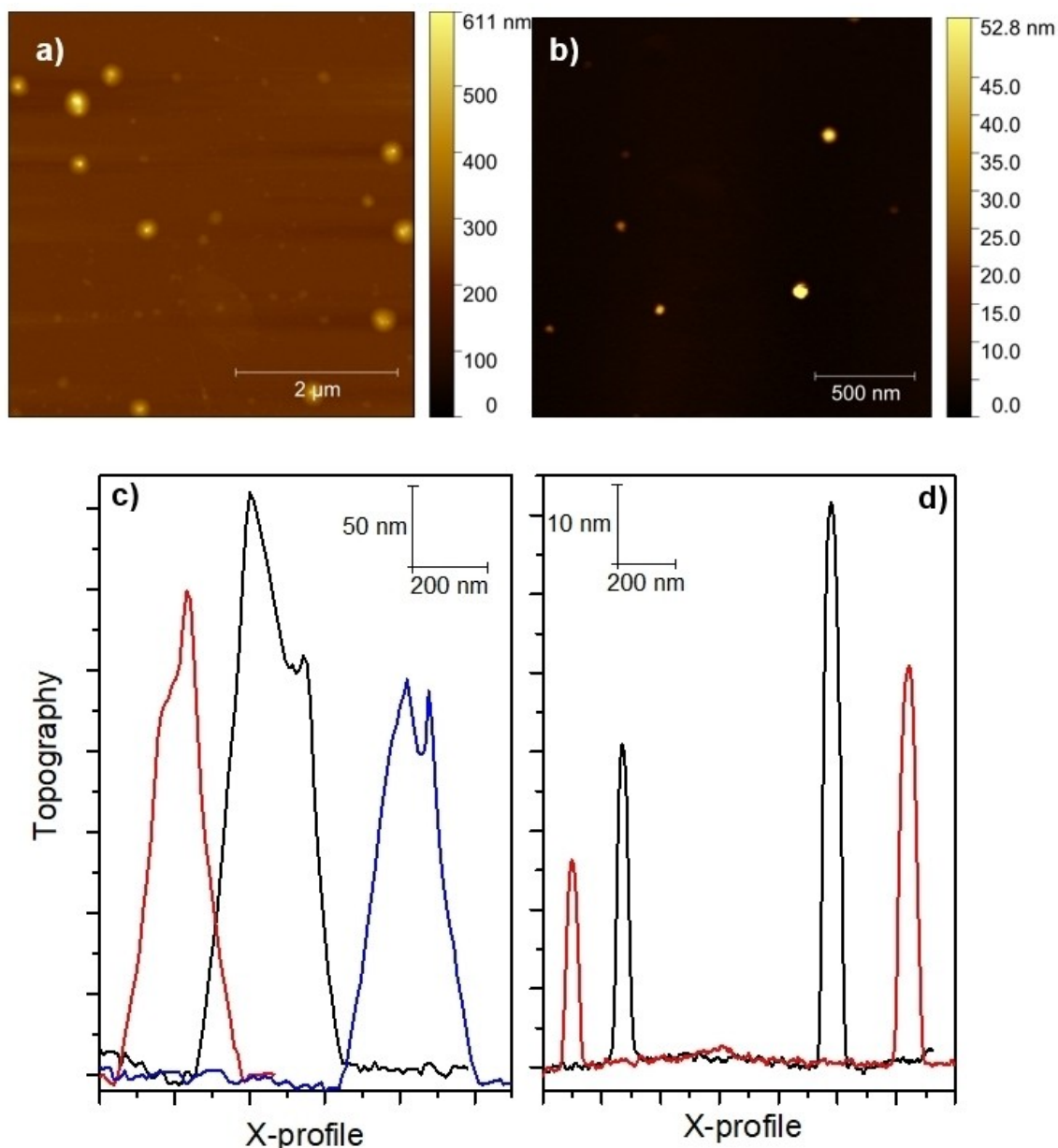


**Figure 5.** AFM topographical images of the typical particle distribution (a) and the “small” fraction (b)  $\text{Sn}^0$  nanoparticles and topographical profiles of agglomerates (c) and “small” fraction (d).

Table 1. The main system characteristics for different reagents (n.d.-not determined) (25 minutes of sonication in THF).				
	Crystallite size (nm) <sup>[a]</sup>	$D_H$ eff (nm) <sup>[b]</sup>	$D_H$ eff (nm) <sup>[c]</sup>	Population (%) <sup>[c]</sup>
1 + $\text{Li}[\text{AlH}_4]$	95	350	130	37
1 + $\text{Na}[\text{BH}_4]$	39	340	140	44
1 + $\text{K}[\text{BEt}_3\text{H}]$	45	280	50	20
2 + $\text{K}[\text{BEt}_3\text{H}]$	59	550	280	50
1 + $\text{K}[\text{BEt}_3\text{H}]$ + PVP40 kDa	n.d.	150	50	80
1 + $\text{K}[\text{BEt}_3\text{H}]$ + PVP360 kDa	n.d.	240	60	40

[a] determined by XRD. [b] The overall colloid and [c] “small” fraction behaviour determined by DLS.

As the reaction of 1 with  $\text{K}[\text{BEt}_3\text{H}]$  yielded the  $\text{Sn}^0$  with the smallest size of crystallites (XRD), we focused on a higher dispersion degree and true nanoparticle colloid preparation from this material by the sonication in THF. Figure 4a presents the time dependency of the particle size distribution of a colloid during sonication. Before sonication, the particles were nonmeasurable by DLS, as they were sedimented due to the size in the order of hundreds of  $\mu\text{m}$  (Figure 1). As can be seen, after 5 minutes of sonication, the trimodal distribution occurred with the “smallest” fraction at the hydrodynamic diameter 180 nm and the fractions at 600 and 1100 nm (the overall effective  $D_H=490$  nm). Due to the further sonication for a cumulative time of 25 minutes, the population of the particles

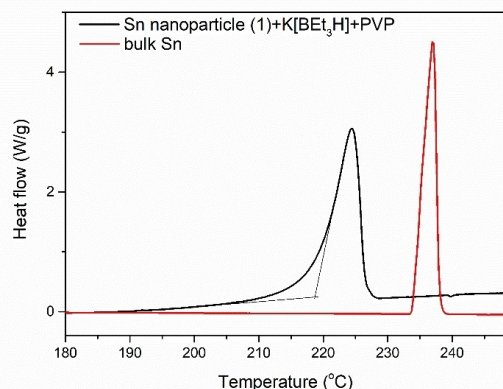


**Figure 6.** Melting DSC curves (endo up) of the as-synthesized Sn<sup>0</sup> nanoparticles prepared by (1) + K[BEt<sub>3</sub>H] stabilized by PVP40 (black) and bulk Sn (red).

600–1100 nm disappeared, being shifted to the distribution of 330 nm, with a smaller size fraction decreasing to around 50 nm (the overall effective  $D_H = 280$  nm). The further sonication (illustrated for 60 min, see Figure 4a) led to an increase in all the parameters of the population (disappearance of the nanoparticles, increase of the overall effective  $D_H = 385$  nm) by the reagglomeration process. This phenomenon was previously observed for other “sticky” nanoparticles in different liquids with different ionic strengths.<sup>[29c,30]</sup>

The unwanted/undesired agglomeration is typically reduced by the surfactant. We used PVP as the most effective stabilizing agent avoiding nanoparticle agglomeration and surface oxidation.<sup>[20–21]</sup> The advantage of PVP as a stabilizing agent is the low influence of the particle growth, wide applications for nanoparticles stabilization and a high affinity to SnO<sub>x</sub>, the disadvantage is a higher crystallite size of prepared Sn<sup>0</sup> particles in comparison with the citrate or hydrobenzamide stabilized particles for a similar synthesis condition (160, and 90 and 50 nm respectively).<sup>[21]</sup> The Sn<sup>0</sup> nanoparticles could also be stabilized by the monomer layer of the new stabilizing agents: 2,4,6-tri(2-pyridyl)-1,3,5-triazine and 3-(2-pyridyl)-5,6-diphenyl-1,2,4-triazine and the stability of the nanoparticles are demonstrated by the successful cycling of the battery with a minimal decrease of the capacity.<sup>[31]</sup> The positive effect of PVP40 kDa was declared on the visual appearance of the colloids (see supplementary materials, Figure S10) and mainly on the histogram (Figure 4b), where the Sn-nanoparticles population is illustrated under a similar procedure as in Figure 4a with the PVP40 kDa addition. The population of nanoparticles dramatically increased (maxima around 50 nm, population over 80%) and the agglomeration process was suppressed. The higher molecular weight PVP360 kDa did not increase the nanoparticle dispersion. This is connected with the decrease in both the solubility of PVP360 kDa and of the molar concentration of accessible PVP for Sn<sup>0</sup> nanoparticles.

By means of the optimization of the process, we were successful in the preparation of the Sn<sup>0</sup> nanoparticles with a

diameter of around 50 nm and narrow size distribution, stable for at least 12 hours (data not shown). Particles around 300 nm were low populated (20%) and there was a need to determine their origin: an agglomerate of the 50 nm nanoparticles or 300 nm single particle. The AFM microscopy and DSC were used for the characterization of the Sn<sup>0</sup> particles. The AFM topographical images indicate the two different sizes of Sn<sup>0</sup> particles synthesized by chemical reduction and stabilized by PVP after 60 min of the sonication. The nanoparticles are round-shaped with the topographical height ranging from 35 to 70 nm (derived from the distance from the substrate, see Figure 5) and the several hundreds nanometers particles (with a height 300–700 nm). The population of the nanoparticles and agglomerates were 72 and 10 units on the scan, respectively. The detection was based on the thresholding technique of image analysis.<sup>[32]</sup> The topographical profiles of agglomerates were not symmetrical (see Figure 5) as a relict of the several crystallites forming these particles. The melting of the dried sample by the DSC confirmed the significant decrease of the melting temperature in comparison with the bulk Sn (220 and 233 °C, determined as an onset temperature, see Figure 6). This is in an agreement with the decrease typical for the 50 nm Sn<sup>0</sup> nanoparticles.<sup>[15a]</sup> The decrease of the minimal melting temperature and increase of the full width at a half maxima is connected with the surface effect of the nanoparticles and size distribution.<sup>[15a]</sup> The PVP presence is displayed as a background shifting during the measurement, not observed on the pure Sn melting (Figure 6).

To the best of our knowledge, based on the observed characteristics of the material (single melting temperature (DSC), the single crystallite size (XRD) and nonsymmetrical agglomerates (AFM)), the agglomerates are formed from 50 nm nanoparticles, in all probability grown from a single nucleus. This results in the stability of the agglomerate during sonication.

## Conclusion

We have demonstrated for the first time a novel way of obtaining a well-dispersed Sn<sup>0</sup> nanoparticles by the reduction of imino-pyridines *N,N*-coordinated Sn<sup>II</sup> complexes. The process was optimized from the point of view of the reducing agent and ligand (K[BEt<sub>3</sub>H] and less shielding complex without Ph group in complex 1), stabilizing agent (PVP40 kDa) and dispersion condition (low-cost sonication) for obtaining stable colloid of 50 nm Sn<sup>0</sup> nanoparticles. The reaction components were characterized by means of <sup>119</sup>Sn{<sup>1</sup>H} NMR spectroscopy and the product by the set of techniques (EDX, XRD, AFM, DSC and DLS).

## Supporting Information Summary

In the Supporting Information the experimental procedures are reported (details of material synthesis, characterization and stabilisation) as well as additional figures.

## Acknowledgements

The financial support from the Czech Science Foundation (GA CR) project No. 19-11814S is highly appreciated. CEMNAT project LM2018103 funded by the Ministry of Youth, Education and Sports of the Czech Republic is acknowledged for the financial support of the SEM measurements provided by Dr. S Šlang. The technical support of Dr. A. Pacinda (Keyence, VHX6000 optical system), assoc. prof. E. Černošková (DSC measurement).

## Conflict of Interest

The authors declare no conflict of interest.

**Keywords:** Chelates · Colloids · Nanoparticles · Reduction · Tin

- [1] a) W. N. C. Weng, *Recent Progress in Soldering Materials* (Ed.: A. A. Mohamad), IntechOpen, **2017**; b) M. Abtew, G. Selvaduray, *Mater. Sci. Eng. R-Rep.* **2000**, *27*, 95–141; c) K. Zeng, K. N. Tu, *Mater. Sci. Eng. R-Rep.* **2002**, *38*, 55–105.
- [2] a) *Solder Materials Market Forecast to 2030*, The Insight Partners, report ID: 5136081 **2020**, p. 147; b) *Solder Materials Market Size, Share & Trends Analysis Report By Product, By Process, By Region, And Segment Forecasts, 2018–2025*, Grand View Research, Report ID: GVR-2-68038-723-0, **2018**, p.78.
- [3] a) S. S. Chee, J. H. Lee, *Thin Solid Films* **2014**, *562*, 211–217; b) A. M. Atieh, T. J. Abedalaziz, A. AlHazzaa, M. Weser, W. G. Al-Kouz, M. S. Sari, I. Alhoweml, *Nanomaterials* **2019**, *9*, 1478.
- [4] a) X. H. Chang, T. Wang, Z. L. Liu, X. Y. Zheng, J. Zheng, X. G. Li, *Nano Res.* **2017**, *10*, 1950–1958; b) Z. Q. Zhu, S. W. Wang, J. Du, Q. Jin, T. R. Zhang, F. Y. Cheng, J. Chen, *Nano Lett.* **2014**, *14*, 153–157.
- [5] A. K. Sinha, A. Sil, A. K. Sasmal, M. Pradhan, T. Pal, *New J. Chem.* **2015**, *39*, 1685–1690.
- [6] A. F. Zatsepina, E. A. Buntov, V. S. Kortov, V. A. Pustovarov, H. J. Fitting, B. Schmidt, N. V. Gavrilov, *J. Surf. Invest.: X-Ray, Synchrotron Neutron Tech.* **2012**, *6*, 668–672.
- [7] a) I. Kityk, J. Ebothe, A. El Hichou, B. Idrissi, M. Addou, J. Krasowski, *J. Opt. A: Pure Appl. Opt.* **2002**, *5*, 61; b) M. Iovu, D. Harea, I. Cojocar, *J. Optoelectron. Adv. Mater.* **2008**, *10*, 3469–3476; c) M. S. Iovu, D. V. Harea, I. Cojocar, E. P. Colomeico, A. Prisacari, V. Ciorba, *J. Optoelectron. Adv. Mater.* **2007**, *9*, 3138–3142.
- [8] Z. Li, X. Tao, Y. Cheng, Z. Wu, Z. Zhang, H. Dang, *Ultrason. Sonochem.* **2007**, *14*, 89–92.
- [9] a) Y. L. Gao, C. D. Zou, B. Yang, Q. J. Zhai, J. Liu, E. Zhuravlev, C. Schick, *J. Alloys Compd.* **2009**, *484*, 777–781; b) C. D. Zou, Y. L. Gao, B. Yang, Q. J. Zhai, C. Andersson, J. Liu, *Solder. Surf. Mt. Technol.* **2009**, *21*, 9–13.
- [10] G. Saito, C. Y. Zhu, T. Akiyama, *Adv. Powder Technol.* **2014**, *25*, 728–732.
- [11] M. Guerrero Correa, F. B. Martínez, C. P. Vidal, C. Streitt, J. Escrig, C. L. de Dicastillo, *Beilstein J. Nanotechnol.* **2020**, *11*, 1450–1469.
- [12] a) M. A. Gondal, Q. A. Drmoh, T. A. Saleh, *Appl. Surf. Sci.* **2010**, *256*, 7067–7070; b) M. Li, Q. H. Lu, Z. G. Wang, *Preparation of tin oxide nanoparticles by laser ablation in solution*, Vol. 5, World Scientific Publ Co Pte Ltd, Singapore, **2006**; c) N. Tarasenko, N. Tarasenko, V. Pankov, *Int. J. Nanosci.* **2019**, *18*, 1940049.
- [13] a) A. B. Yaroslavtsev, Y. A. Dobrovolsky, N. S. Shaglaeva, L. A. Frolova, E. V. Gerasimova, E. A. Sanginov, *Russ. Chem. Rev.* **2012**, *81*, 191–220; b) T. Ramulifho, K. I. Ozoemena, R. M. Modibedi, C. J. Jafta, M. K. Mathe, *Electrochim. Acta* **2012**, *59*, 310–320.
- [14] S.-S. Chee, J.-H. Lee, *Electron. Mater. Lett.* **2012**, *8*, 587–593.
- [15] a) H. Jiang, K.-s. Moon, H. Dong, F. Hua, C. P. Wong, *Chem. Phys. Lett.* **2006**, *429*, 492–496; b) C.-d. Zou, Y.-l. Gao, B. Yang, Q.-j. Zhai, *Trans. Nonferrous Met. Soc. China* **2010**, *20*, 248–253; c) H. Zhang, H. Song, X. Chen, J. Zhou, *J. Chem. Phys. C* **2012**, *116*, 22774–22779.
- [16] A. L. Caballero, J. N. Morales, L. Sánchez, *Electrochem. Solid-State Lett.* **2005**, *8*, A464.
- [17] L. Balan, R. Schneider, D. Billaud, J. Ghanbaja, *Mater. Lett.* **2005**, *59*, 1080–1084.
- [18] L. E. Depero, E. Bontempi, L. Sangaletti, S. Pagliara, *J. Chem. Phys.* **2003**, *118*, 1400–1403.
- [19] H.-m. Xie, X.-d. Van, H.-y. Yu, L.-y. Zhang, G.-l. Yang, Y. Xu, R.-s. Wang, *Chem. Res. Chin. Univ.* **2006**, *22*, 639–642.
- [20] S.-S. Chee, J.-H. Lee, *Electron. Mater. Lett.* **2012**, *8*, 53–58.
- [21] Y. Kwon, M. G. Kim, Y. Kim, Y. Lee, J. Cho, *Electrochem. Solid-State Lett.* **2006**, *9*, A34.
- [22] C. Nayral, E. Viala, P. Fau, F. Senocq, J.-C. Jumas, A. Maisonnat, B. Chaudret, *Chem. Eur. J.* **2000**, *6*, 4082–4090.
- [23] a) S. Khan, P. P. Samuel, R. Michel, J. M. Dieterich, R. A. Mata, J.-P. Demers, A. Lange, H. W. Roesky, D. Stalke, *Chem. Commun.* **2012**, *48*, 4890–4892; b) L. W. Pineda, V. Jancik, K. Starke, R. B. Oswald, H. W. Roesky, *Angew. Chem. Int. Ed.* **2006**, *45*, 2602–2605; *Angew. Chem.* **2006**, *118*, 2664–2667.
- [24] a) R. E. Murray, *PCT Int. Appl., WO1999001460 A1* **1999**; b) M. Novák, H. Hošnová, L. Dostál, B. Glowacki, K. Jurkschat, A. Lyčka, Z. Ruzickova, R. Jambor, *Chem. Eur. J.* **2017**, *23*, 3074–3083.
- [25] M. Ibarra-Rodriguez, B. M. Munoz-Flores, H. V. R. Dias, I. F. Hernandez-Ahuactzi, M. Sanchez, V. M. Jimenez-Perez, *Arabian J. Chem.* **2019**, *12*, 5120–5124.
- [26] W. Grochala, P. P. Edwards, *Chem. Rev.* **2004**, *104*, 1283–1316.
- [27] a) P. Debye, P. Scherrer, *P. Physik. Z.* **1916**, *17*, 277–283; b) U. Holzwarth, N. Gibson, *Nat. Nanotechnol.* **2011**, *6*, 534–534; c) R. Todorov, V. Lozanova, P. Knotek, E. Černošková, M. Vlček, *Thin Solid Films* **2017**, *628*, 22–30.
- [28] EVA SW; ver. 19 ed., Bruker AXS GmbH, Germany, **2013**.
- [29] a) Å. K. Jamting, J. Cullen, V. A. Coleman, M. Lawn, J. Herrmann, J. Miles, M. J. Ford, *Adv. Powder Technol.* **2011**, *22*, 290–293; b) M. A. Al-Khafaji, A. Gaál, A. Wacha, A. Bóta, Z. Varga, *Materials* **2020**, *13*, 3101; c) A. L. Poli, T. Batista, C. C. Schmitt, F. Gessner, M. G. Neumann, *J. Colloid Interface Sci.* **2008**, *325*, 386–390.
- [30] a) J. Oprsal, L. Blaha, M. Pouzar, P. Knotek, M. Vlcek, K. Hrda, *Environ. Sci. Pollut. Res. Int.* **2015**, *22*, 19124–19132; b) I. Au-Kaur, L.-J. Au-Ellis, I. Au-Romer, R. Au-Tantra, M. Au-Carriere, S. Au-Allard, M. Au-Mayne-L'Hermite, C. Au-Minelli, W. Au-Unger, A. Au-Potthoff, S. Au-Rades, E. Au-Valsami-Jones, *JoVE* **2017**, e56074.
- [31] M. Noh, Y. Kim, M. G. Kim, H. Lee, H. Kim, Y. Kwon, Y. Lee, J. Cho, *Chem. Mater.* **2005**, *17*, 3320–3324.
- [32] a) P. K. Sahoo, S. Soltani, A. K. C. Wong, *Computer Vision, Graphics, and Image Processing* **1988**, *41*, 233–260; b) P. Knotek, M. Vlcek, M. Kincl, L. Tichy, *Thin Solid Films* **2012**, *520*, 5472–5478; c) E. Bílková, M. Sedlák, B. Dvořák, K. Ventura, P. Knotek, L. Beneš, *Org. Biomol. Chem.* **2010**, *8*, 5423–5430.

Submitted: February 18, 2021

Accepted: April 12, 2021